Chirality

WILEY

Chirality

RESEARCH ARTICLE OPEN ACCESS

Inherently Chiral Oligomers Based on Indole–Benzothiophene Core

Bartlomiej Bonczak[1] | Sara Grecchi[1] | Malinee Niamlaem[1] | Gerardo Salinas[2] | Roberto Cirilli[3] | Serena Arnaboldi[1]

[1]Dip. Di Chimica, Univ. degli Studi di Milano, Milan, Italy | [2]Univ. Bordeaux, CNRS, Bordeaux INP, ISM, UMR 5255, Pessac, France | [3]Istituto Superiore di Sanità, Centro Nazionale per il Controllo e la Valutazione dei Farmaci, Rome, Italy

Correspondence: Serena Arnaboldi (serena.arnaboldi@unimi.it)

Received: 14 May 2024 | **Revised:** 15 July 2024 | **Accepted:** 17 July 2024

Funding: This work has been funded by the H2020 European Research Council (ERC) under the HORIZON-ERC-2021 work program (grant agreement no. 101040798, ERC Starting grant CHEIR).

Keywords: chiral recognition | conducting polymers | in situ electrochemical conductance | inherently chiral oligomers

ABSTRACT

In recent years, transductors of chiral information based on conducting polymers have gained considerable attention. In particular, inherently chiral materials, which allow differentiation between the antipodes of a chiral analyte in terms of energetic variations, are highly desired. In this work, we successfully synthesized a novel inherently chiral oligomer based on an indole–benzothiophene core, namely, 2-([2,2′-bithiophen]-5-yl)-3-(2-([2,2′-bithiophen]-5-yl)benzo[*b*]thiophen-3-yl)-*N*-methylindole ($BTIndT_4$). The electrochemical characterization evidences a stabilization of electrogenerated radical cations due to the presence of the indole group, which guides the oligomerization, producing well-ordered polymeric matrices. Furthermore, the in situ electrochemical conductance analysis demonstrates a simultaneous intrachain and interchain transfer of charge carriers. Finally, the highly efficient enantiorecognition capabilities of the antipodes of the oligo-$BTIndT_4$ films toward the enantiomers of tryptophan and 3,4-dihydroxyphenylalanine (DOPA), as model chiral analytes, were demonstrated.

1 | Introduction

Conducting polymers are versatile materials that have gained considerable attention in multiple applications ranging from electrostatic coatings to energy storage and sensing [1–4]. Recently, these highly π-conjugated systems have become an interesting alternative as transducers of physicochemical information. The novel functionality arises from modifying the oligomeric chain with active moieties or templating the bulk of the polymeric network with a selective cavity [5–9]. With this philosophy, multiple electroactive polymeric systems have been designed to serve as electrochemical transductors of chiral information [10–14]. The design of enantioselective electrode surfaces is of utmost importance in various fields, such as chiral separation, asymmetric synthesis, and sensing [15–21]. However, the functionalization and templating approaches lack real enantioselectivity since the differentiation between the antipodes of a chiral analyte is commonly achieved by detecting kinetic changes (i.e., current). It presents a difficulty for the electrochemical studies of enantiomeric mixtures because the redox process can occur at the same electrode potential.

In this context, inherently chiral oligomers have become a powerful tool for discriminating electroactive enantiomers [22]. The enantioselectivity mechanism of these π-conjugated materials is based on favorable or unfavorable diastereomeric interactions between the chiral oligomeric surface and the antipodes of an analyte. Such a particular effect leads to an energetic differentiation, expressed by relatively significant thermodynamic potential differences between the two enantiomers [22]. The keystone of enantioselectivity, from a structural point of view, lies in the coincidence of the stereogenic and electroactive elements within

the polymeric backbone. Although different types of inherently chiral oligomers based on biindole and helicene cores have been designed [23–25], the benchmark of this type of material is the 2,2′-di([2,2′-bithiophen]-5-yl)-3,3′-bibenzo[*b*]thiophene (BT_2T_4) [26].

Multiple electrochemical systems for the transduction of chiral information in solution have been developed by taking advantage of the outstanding enantioselective capabilities of BT_2T_4 [27–30]. However, the design of alternative inherently chiral monomers and their corresponding oligomers, capable of highly efficient enantiorecognition, is still underway.

In this work, we present the synthesis and the electrochemical properties of both a novel inherently chiral monomer based on an indole–benzothiophene core, namely, 2-([2,2′-bithiophen]-5-yl)-3-(2-([2,2′-bithiophen]-5-yl)benzo[*b*]thiophen-3-yl)-*N*-methylindole ($BTIndT_4$), and the corresponding oligomeric films. The indole moiety within the stereogenic core provides additional stabilization of charges, guiding the electrooligomerization to produce a well-ordered polymer matrix, as reflected by the potentiodynamic and in situ conductance profiles. In addition, the enantioselective capability of the oligomers of both enantiomers of $BTIndT_4$ (oligo-(*S*)- and oligo-(*R*)-, Figure 1a), toward the antipodes of tryptophan (Try) and 3,4-dihydroxyphenylalanine (DOPA), was evaluated.

2 | Materials and Methods

2.1 | Synthesis of $BTIndT_4$

2.1.1 | Synthesis of 3-Bromo-*N*-Methylindole (3)

A Br_2 (2.762 g, 17.286 mmol, 0.89 mL, 1.01 eq) solution in dimethylformamide (DMF) (25 mL) was dropwise added to a reaction flask containing indole (**1**) (2.00 g, 17.072 mmol) in DMF (25 mL). After completion, the reaction was poured onto a mixture of water (600 mL), ice, NH_3 (0.5%), and Na_2SO_4 (0.1%). The precipitate was filtered, washed with cold water, and dried on air. The crude 3-bromoindole (**2**) (4.179 g, > 100% slightly wet) in the form of a beige solid was used immediately in the next step without further purification. ^{1}H NMR (300 MHz, $CDCl_3$, δ): 8.19 (s, 1H), 7.65–7.53 (m, 1H), 7.43–7.36 (m, 1H), 7.31–7.15 (m, 3H) ppm. 3-Bromoindole (**2**) from the previous step was dissolved in DMF (15 mL), and grounded KOH (1.34 g, 23.90 mmol, 1.40 eq) was added in portions under argon atmosphere. When most of the solid dissolved, the mixture was cooled to 0°C (water-ice bath), and methyl iodide (1.17 mL, 18.78 mmol, 1.10 eq) was dropwise added over 40 min. The cooling bath was removed, and the reaction was stirred for 1 h at room temperature until the TLC showed complete substrate consumption. The reaction was quenched with water (200 mL), and the mixture was extracted with diethyl ether (3 × 30 mL). The combined organic extracts were washed with water (30 mL) and brine (10 mL) and dried with Na_2SO_4. The filtered solution was concentrated with one drop of triethyl amine as a stabilizer. The resulting tan oil (3.34 g, 93% over two steps) was used in the next step without further purification. ^{1}H NMR (300 MHz, $CDCl_3$, δ) 7.62–7.52 (m, 1H), 7.36–7.24 (m, 2H), 7.23–7.16 (m, 1H), 7.07 (s, 1H), 3.78 (s, 3H) ppm. ^{13}C NMR (75 MHz, $CDCl_3$, δ) 136.29, 127.68, 127.30, 122.62, 120.09, 119.30, 109.44, 89.35, 33.03 ppm.

2.1.2 | Synthesis of *N*-Methyl-3-(3-Benzo[*b*]thienyl) indole (4)

3-Bromo-*N*-methylindole (**3**) (1500 mg, 7.619 mmol), benzo[*b*]thien-3-ylboronic acid (**3-BBT**) (1493.5 mg, 8.380 mmol, 1.10 eq), Pd $(OAc)_2$ (34.1 mg, 0.152 mmol, 2% mol), and *t*$Bu_3P{\cdot}HBF_4$ (53.1 mg, 0.183 mmol, 2.4% mol) were introduced into a Schlenk flask which was then evacuated and filled with argon three times. Dry dioxane (20 mL) and crusher NaOH (518.1 mg, 12.95 mmol, 1.7 eq) were added to the reaction mixture. The reaction was run for 8 h at room temperature. During that time, the color of the mixture changed from yellow to orange and black. Once TLC showed the total consumption of (**3**), the mixture was diluted with DCM (30 mL), and silica gel was added. The mixture was concentrated to dryness and applied on a short chromatographic column eluted with hexane to remove nonpolar impurities, and then, hexane:EtOAc (90:1–30:1) to elute the product (**4**) (1.889 g, 94%) in the form of a colorless, crystalline solid. ^{1}H NMR (300 MHz, $CDCl_3$, δ) 8.01–7.94 (m, 2H), 7.78 (d, J = 7.9 Hz, 1H), 7.50 (s, 1H), 7.46–7.38 (m, 3H), 7.38–7.30 (m, 2H), 7.25–7.16 (m, 1H), 3.90 (s, 3H) ppm. ^{13}C NMR (75 MHz, $CDCl_3$, δ) 140.56, 138.89, 137.17, 131.01, 127.41, 124.45, 124.17, 123.46, 122.99, 122.31, 122.23, 120.36, 119.89, 110.51, 109.61, 77.16, 33.05 ppm.

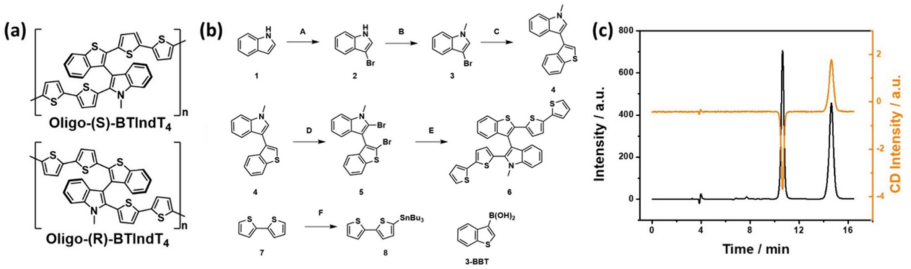

FIGURE 1 | (a) Chemical structures of the oligo-(*S*)- and oligo-(*R*)-2-([2,2′-bithiophen]-5-yl)-3-(2-([2,2′-bithiophen]-5-yl)benzo[b]thiophen-3-yl)-*N*-methylindole ($BTIndT_4$). (b) Schematic illustration of the synthetic steps followed for the synthesis of $BTIndT_4$ with a representation of the corresponding intermediaries: (A) Br_2, DMF, rt; (B) MeI, DMF, rt, 93% over two steps; (C) 3-BBT, Pd $(OAc)_2$ (2%), *t*-$Bu_3P{\cdot}HBF_4$ (2.4%), NaOH, dioxane, rt, 94%; (D) NBS, DMF, rt, 71%; (E) 8, Pd $(PPh_3)_4$ (5%), toluene, 100°C, 69%; (F) 1. BuLi (2.5 M), THF, −78°C, 2. Bu_3SnCl, −78°C to rt. (c) Chromatogram (left axis black line) with online UV (black line)/CD (orange line) detection at 360 nm of the racemic $BTIndT_4$.

2.1.3 | Synthesis of 2-Bromo-3-(2-Bromobenzo[*b*] thiophen-3-Yl)-*N*-Methylindole (5)

A solution of (**4**) (263.0 mg, 1.00 mmol) in DMF (10 mL) was treated with a solution of NBS (*N*-bromosuccinimide) (355.6 mg, 2.00 mmol) in DMF (15 mL) at 0°C introduced dropwise over 40 min. The reaction was stirred for 1 h at room temperature until completion (followed by TLC). The reaction was then quenched with water (150 mL) and extracted with DCM (3 × 20 mL). Combined organic phases were washed with water (2 × 20 mL), dried with Na_2SO_4, filtered, and concentrated. The crude product was purified with column chromatography (hexane to hexane:EtOAc, 60:1) to give the product in the form of a colorless crystalline solid (299.6 mg, 71%). ^{1}H NMR (300 MHz, $CDCl_3$, δ) 7.82 (d, J = 7.9 Hz, 1H), 7.47–7.25 (m, 6H), 7.13 (t, J = 7.5 Hz, 1H), 3.92 (s, 3H) ppm. ^{13}C NMR (75 MHz, $CDCl_3$, δ) 139.87, 138.96, 137.03, 130.18, 127.24, 124.80, 124.67, 123.67, 122.46, 121.87, 120.49, 119.82, 116.05, 115.18, 109.79, 108.96, 77.16, 31.98 ppm. MS (MALDI-TOF-TOF) m/z: $[M]^+$ calculated for $C_{17}H_{11}N_SBr_2$, 420.897; found, 420.911.

2.1.4 | Synthesis of 5-Tributylstannyl-2,2′-Bithiophene (8)

Bithiophene (**7**) (352.0 mg, 2.117 mmol, 1.00 eq) was introduced into a Schlenk tube, which was evacuated and filled with argon three times. Dry THF (5.0 mL) was added to form a solution, which was then cooled to −78°C (dry ice/isopropanol bath). BuLi (0.85 mL, 2.117 mmol, 1.00 eq, 2.5 M in hexane) was dropwise added over 15 min. The reaction was stirred at −78°C for 1 h, and then, Bu_3SnCl (0.60 mL, 2.223 mmol, 1.05 eq) was dropwise added. After 20 min, the cooling bath was removed, and the mixture was left to react overnight (about 14 h) at room temperature. After this time, the reaction was quenched with a saturated solution of NH_4Cl (~15 mL). The mixture was extracted with diethyl ether (3 × 20 mL), and combined organic washes were dried with Na_2SO_4. The filtrated solution was concentrated to dryness, giving the crude product (1.00 g) as a dark oil, which was used in the next step without further purification.

2.1.5 | Synthesis of $BTIndT_4$ (6)

A Schlenk tube was charged with (**5**) (105.0 mg, 0.250 mmol, 1.00 eq) and 5-tri-n-butylstannyl-2,2′-bithiophene (**8**) (342.0 mg, 0.750 mmol, 3.00 eq). The flask was evacuated and filled with argon three times; afterward, dry toluene was added (3.0 mL). Finally, Pd $(PPh_3)_4$ (11.0 mg, 0.010 mmol, 4% mol) was added, and the reaction was heated to 90°C and run overnight (about 14 h). After that time, TLC showed no full consumption of substrate, therefore an additional portion of (**8**) (100 mg, 0.220 mmol, 0.88 eq) was added, and after 4 h, the reaction was completed (followed by TLC). The reaction was cooled to room temperature and quenched with a mixture of KF (~100 mg) and acetone (~10 mL). The resulting slurry mixture was stirred vigorously for an hour, and precipitated solids were filtered through celite. Filtrate was concentrated with silica gel, and (**6**) was separated using a chromatographic column eluted with hexane to remove nonpolar impurities and then hexane:EtOAc (90:1 to 30:1) to elute the product (101.4 mg, 69%) in the form of a yellow solid. ^{1}H NMR (300 MHz, $CDCl_3$, δ) 7.80 (d, J = 7.8 Hz, 1H), 7.49 (d, J = 8.1 Hz, 1H), 7.39–7.26 (m, 3H), 7.26–7.17 (m, 2H), 7.16–7.06 (m, 3H), 7.02–6.98 (m, 1H), 6.97–6.89 (m, 6H), 6.75 (d, J = 3.6 Hz, 1H), 3.97 (s, 3H) ppm. ^{13}C NMR (75 MHz, $CDCl_3$, δ) 141.97, 139.25, 138.41, 138.33, 137.96, 137.35, 137.01, 135.64, 135.20, 132.66, 130.75, 129.16, 127.98, 127.90, 127.85, 127.05, 125.87, 124.84, 124.65, 124.62, 124.54, 124.00, 123.81, 123.76, 123.72, 122.98, 122.00, 120.58, 120.30, 109.82, 108.95, 77.16, 31.81 ppm. MS (MALDI-TOF-TOF) m/z: $[M]^+$ calculated for $C_{33}H_{21}NS_5$, 591.027; found, 591.032.

2.1.6 | Enantioselective High-Performance Liquid Chromatography

HPLC-grade solvents were provided by Aldrich (Milan, Italy). HPLC enantioseparations were performed on stainless steel Chiralpak IB 250 × 4.6 mm, 5 μm, and Chiralpak IB 250 mm × 10 mm, 5 μm, columns (Chiral Technologies Europe, Illkirch-Graffenstaden, France). The analytical HPLC apparatus consisted of a PerkinElmer 200 LC pump equipped with a Rheodyne injector, a 50-μL sample loop, an HPLC Dionex CC-100 oven, and a Jasco model CD 2095 Plus UV/CD detector. For semipreparative resolutions, a PerkinElmer 200 LC pump equipped with a Rheodyne injector, a 2-mL sample loop, a PerkinElmer LC 101 oven, and a Waters 484 detector were used. Clarity software from DataApex was used to acquire and process the signal.

2.1.7 | Electronic Circular Dichroism (ECD) Measurements

The ECD spectra of the enantiomers of $BTIndT_4$ collected on a semipreparative scale were recorded in chloroform at 25°C using a Jasco Model J-700 spectropolarimeter. The optical path was 1 mm. The spectrum average is computed over four instrumental scans, and the intensities are presented in terms of ellipticity values (millidegrees).

2.2 | Electrochemical Methods

2.2.1 | Potentiodynamic Oligomerization and Characterization

Electrodeposition was carried out in a 0.1 M $LiClO_4$ ACN solution containing 0.75 mM of $BTIndT_4$ monomer by cyclic voltammetry. A glassy carbon electrode (GC, A = 0.033 cm^2) was used as a working electrode with a Pt mesh and Ag/AgCl as counter and reference electrodes, respectively. After deposition, the redox behavior of the modified electrode was evaluated potentiodynamically in a free-monomer 0.1 M $LiClO_4$ ACN. A three-electrode cell composed of the modified GC electrode, a Pt mesh, and an Ag/AgCl, acting as working, counter, and reference electrodes, was used. All the electrochemical measurements were performed using a PalmSens potentiostat connected to a personal computer.

2.2.2 | In Situ Electrochemical Conductance Method

Interdigital microarray electrodes (IDMAEs) of 1 cm × 0.5 cm, with Pt bands separated by 10 μm, were used as working electrodes. A three-electrode electrochemical cell fitted with a Pt foil and an Ag wire, acting as counter and pseudoreference electrodes, respectively, and the IDMAE was used. In situ electrochemical conductance measurements were carried out using a two-potentiostat system connected to a symmetry unit specially built for this method. For this, a PalmSens and an Autolab were connected individually to a personal computer. With one potentiostat, a constant potential difference (ΔV) of 10 mV is applied between the IDMAE branches, obtaining the correspondent drain current. From this, the conductance was estimated according to Ohm's law. The second potentiostat is used to evaluate the classic electrochemical characterization. More details concerning this technique can be found elsewhere in the literature [31, 32].

2.2.3 | Enantioselective Capability

The potentiodynamic characterizations of the chiral probes were carried out in a classic three-electrode cell coupled with an unmodified or modified GC working electrode, Pt mesh, Ag/AgCl counter, and reference electrodes. The chiral probes were dissolved individually in a commercial pH 4 buffer solution (Fluka, prepared with citric acid, NaOH, and NaCl). The D- and L-enantiomers of Try and 3,4-DOPA were used as model chiral analytes.

3 | Results and Discussion

3.1 | Synthesis of $BTIndT_4$ Monomers

The synthetic strategy was based on the functionalization of the 3-(benzo[*b*]thiophen-3-yl)-1-methyl-1*H*-indole (**4**) to introduce bithiophene units to the main structure. Such modification provides oligomerization sites to the core and blocks the rotation of the C-C bond between indole and benzothiophene units. The schematic illustration of the synthetic steps with the corresponding products is depicted in Figure 1b. At first, the bromination of indole (**1**), following a procedure previously established, was carried out [33]. Afterwards, the brominated indole (**2**) was immediately used, without further purification, for the *N*-methylation step. Then, via a Suzuki–Miyaura cross-coupling reaction between the 3-bromo-N-methylindole (**3**) and the **3-BBT**, the N-methyl-3-(3-benzo[b]thienyl)indole (**4**) was successfully obtained with an excellent yield of 94% [34]. In the next step, the corresponding bromination of the 2 and 2′ positions of (**4**) was performed using NBS as the bromine source in DMF. Under these conditions, the 2-bromo-3-(2-bromobenzo[b]thiophen-3-yl)-N-methylindole (**5**) was produced with a good (71%) yield. Finally, utilizing a Stille cross-coupling reaction [26] between the 5-tri-n-butylstannyl-2,2′-bithiophene (**8**) [35] and compound (**5**), the $BTIndT_4$ (**6**) was obtained with a yield of 69% in the form of a yellow solid. The spectroscopic data of compounds (**2**) [33], (**3**) [36], and (**4**) [34] matched those reported in the literature. Spectroscopic data of compounds (**5**) and (**6**) are presented in the supporting information (Figures S1–S6).

The separation of the enantiomers of $BTIndT_4$ was achieved by HPLC on the immobilized type cellulose-based Chiralpak IB chiral stationary phase. Figure 1c shows the optimized resolution obtained with the eluent mixture *n*-hexane-DEA-MeOH-DCM 100:0.1:0.5:0.5 and a column temperature of 15 °C. The 25 mm × 10 mm Chiralpak IB column was used to scale up the enantioselective analytical conditions to a semi-preparative level and to collect multimilligram amounts of enantiopure forms (ee > 99.0%). The absolute configuration of the isolated enantiomers was determined empirically by ECD correlation. The enantiomers of the chiral analog BT_2T_4 were used as a reference because their stereochemistry has been established in previous work [22]. As highlighted by the ECD spectra shown in Figure S7, the (*S*) enantiomer of BT_2T_4 shares a strong positive Cotton effect in the 500–300 nm spectral region with the first eluted enantiomer of $BTIndT_4$. This means that the enantiomers of the two atropisomeric compounds have the same (*S*) configuration. An (*R*) configuration can be assigned to the more retained enantiomer of $BTIndT_4$. It is noteworthy that at the diagnostic wavelength of 360 nm, there is a clear correlation between the sign of the online CD peak obtained during the enantioselective HPLC (Figure 1c) and the absolute configuration (i.e., the negative online CD signal corresponds to the (*S*) configuration and vice versa). Thus, the stereochemistry of the enantiomers of these atropisomers can be directly deduced from the sign of the HPLC CD detector.

3.2 | Electrochemical Characterization

The electrochemical characterization was performed after synthesizing and separating the $BTIndT_4$ enantiomers. At first, the potentiodynamic oxidation of $BTIndT_4$ in a 0.75 mM monomer, 0.1 M $LiClO_4$ ACN solution, was performed (Figure S8). It exhibits two redox processes associated with the oxidation/reduction of the indole–benzothiophene core ($I_a/I_c \approx 1.0$ V vs. Ag/AgCl) and the charge/discharge of the bithiophene extremities ($II_a/II_c \approx 1.1$ V vs. Ag/AgCl). Due to the highly conjugated structure of the monomer, the radical cations, which formed at these potential values, are relatively stable, thus limiting the oligomerization process. Therefore, the electro-oligomerization of the monomer was carried out at potential values above 1.2 V versus Ag/AgCl to enrich the electrode's surface with the oxidized form of $BTIndT_4$, favoring polymerization. As expected under these conditions, a gradual increase in the current of both peaks was observed, indicating the surface modification of the electrode with the oligo-$BTIndT_4$ (Figure 2) [37]. However, after 36 cycles of electro-oligomerization, both redox systems merge into a single quasireversible peak. This is a characteristic feature of $BTIndT_4$, in contrast to the electrochemical oligomerization of BT_2T_4; during which, similarly to polythiophene, only cathodic peaks are defined [38].

The electrochemical behavior of the obtained films was evaluated in a monomer-free 0.1 M $LiClO_4$ ACN solution by sweeping in a range of potentials where the polymer is electroactive and stable (between 0 and 1.3 V vs. Ag/AgCl). The potentiodynamic plot exhibits a quasimirror voltammetric signal between the anodic and cathodic current, with a potential difference between the main peaks of ≈120 mV (Figure S9).

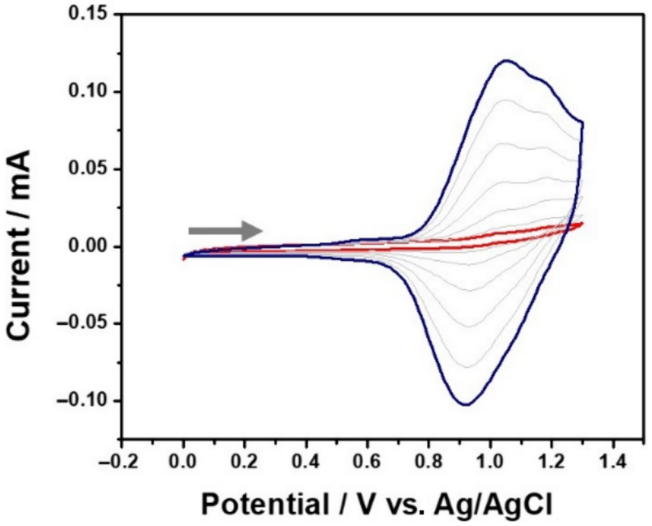

FIGURE 2 | Potentiodynamic oligomerization (36 cycles) of $BTIndT_4$ 0.75 mM, obtained in a 0.1 M $LiClO_4$ ACN solution, v = 0.2 V/s; WE:GC. The red and blue lines indicate the 1st and 36th cycles, respectively.

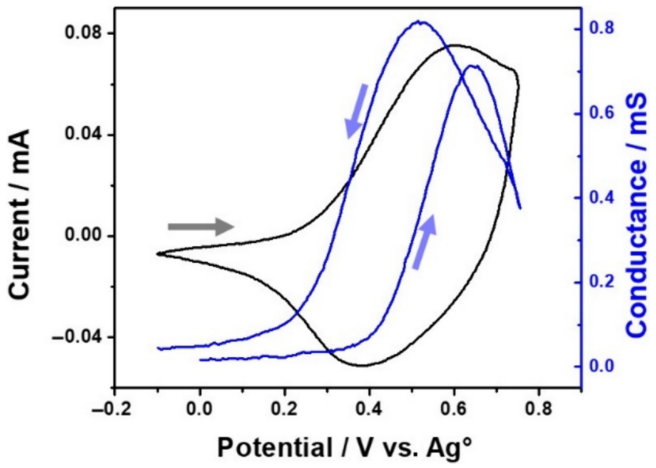

FIGURE 3 | Electrochemical (left axis black line) and conductance (right axis blue line) simultaneous study of an oligo-$BTIndT_4$ film obtained in a monomer-free solution, 0.1 M $LiClO_4$ ACN, v = 0.05 V/s, WE:Pt IDME, ΔV = 10 mV.

These features are close to the theoretical voltammetric signal associated with thin-layer films with fast electron-kinetics exchange [39]. Furthermore, the quasimirror response, in contrast with the electrochemical behavior of poly-3,4-ethylene dioxythiophene (PEDOT) or poly-bithiophene (PBTh), is associated with the possible formation of a well-ordered internal polymer matrix [40]. Once again, such a symmetric electrochemical response is characteristic of the oligo-$BTIndT_4$ since alternative inherently chiral oligomers, such as oligo-BT_2T_4 or 3,3′-bithianaphthene cores decorated with EDOT (nicknamed BT_2E_4), exhibit two voltammetric signals [38]. This is interesting since the intrachain and interchain transfer of charge carriers within oligo-$BTIndT_4$ co-occur (at the same potential), whereas for oligo-BT_2T_4 and oligo-BT_2E_4 occur at rather different potentials [31].

In situ electrochemical conductance experiments were carried out to provide a deeper understanding of the charge/discharge process of this new inherently chiral oligomer. As can be seen in Figure 3 (blue axis), a well-shaped conductance profile for the anodic and cathodic sweeps, reaching a maximum of around 0.7 and 0.8 mS, respectively, was obtained. The bell-shaped conductance profile commonly agrees with redox polymers' mixed valence conductivity characteristic [31]. In these systems, the charge transport occurs via a charge hopping mechanism between localized redox sites. Although such observations were made for oligo-BT_2T_4 and oligo-BT_2E_4 [38], no other conductance signals were obtained at potentials below the main redox systems of the oligo-$BTIndT_4$. Additional conductance signals at relatively low potential values are commonly associated with alternative insulating/conducting transitions [31]. Thus, these results corroborate the assumption that during the charge/discharge process, the intrachain and interchain transfer of charge carriers within oligo-$BTIndT_4$ occurs simultaneously. In addition, in the case of the obtained films, the insulating/conducting transitions occur at two different potentials. This can be attributed to the indole–thianaphthene core stabilizing the electrochemically produced charges. Thus, higher energy is required to reduce the charged cores. In synergy with the voltammetric profile, which is characteristic of a quasireversible charge transfer, the hysteresis of the conductance (evaluated at the half-wave G vs. E plot) is relatively low ($\Delta E_G = 180$ mV), in comparison with kinetically slow systems such as PEDOT or PBTh ($\Delta E_G > 300$ mV) [40]. Once again, this is attributed to the formation of a well-ordered internal polymer matrix during the electropolymerization.

3.3 | Enantioselective Capability

In the next step, the enantioselective capabilities of these novel inherently chiral films were tested. For this purpose, the two antipodes of the chiral film, namely, oligo-(*R*)- or oligo-(*S*)-$BTIndT_4$, were tested independently in a buffer solution (at pH 4) containing 4 mM of a given enantiomer of Try. As can be seen in Figure 4a, the voltammetric response of an unmodified GC electrode for both enantiomers of Try exhibits a single oxidation peak around 0.9 V versus Ag/AgCl. However, by using the oligo-(*R*)-electrode, the oxidation of L-Try shifts toward higher anodic potentials (1.7 V vs. Ag/AgCl), whereas the oxidation peak of the D-enantiomer appears at a similar potential value of the one recorded on bare GC electrode (Figure 4b). Such rather large peak-to-peak separation (around 700 mV) indicates that the oligo-(*R*)-film inhibits the electron transfer during the oxidation of L-Try. Thus, it is possible to assume that an unfavorable diastereomeric interaction between the (*R*)-oligomer and the L-probe occurs. In addition, the specular voltammetric response was obtained when using the oligo-(*S*)-film; thus, this oligomer inhibits the oxidation of the D-Try (Figure 4c). Although shifts toward lower oxidation potential values were expected for the favorable diastereomeric interactions, electron transfer inhibition has been observed for the oxidation of different chiral analytes, such as doxorubicin and the antipodes of limonene and carvone, by using BT_2T_4 films [41].

Finally, we evaluated the broadness of the enantioselectivity of these materials by using an alternative chiral probe, that is,

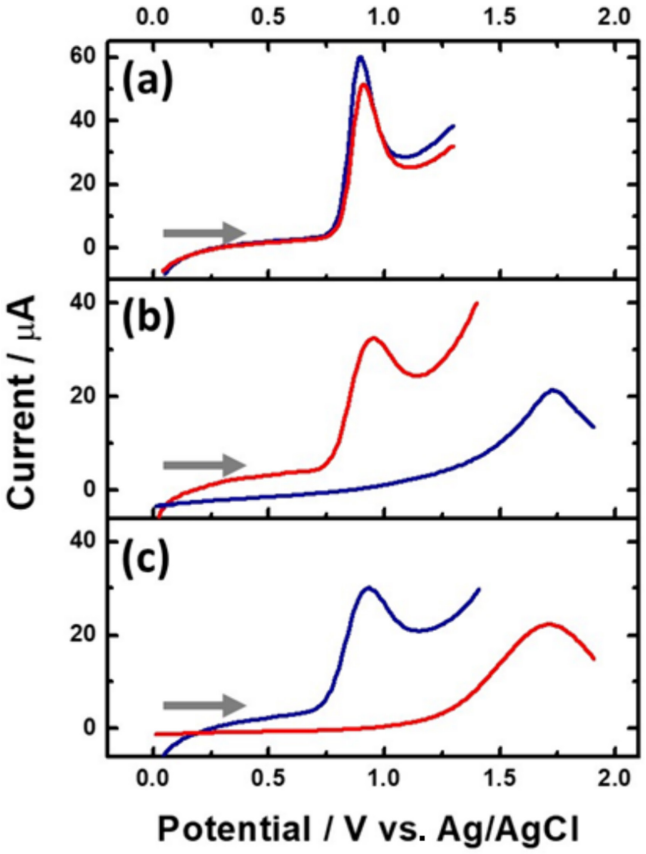

FIGURE 4 | Potentiodynamic enantioselectivity test for D- and L-Try (red and blue lines, respectively) obtained on (a) an unmodified and modified GC electrode with (b) oligo (*R*)- and (c) oligo-(*S*)-BTIndT$_4$, in a 4 mM chiral probe, pH 4 buffer solution, v = 0.05 V/s.

DOPA. In this case, the redox process of D- of L-DOPA was tested independently (and together as a racemate, 50:50 L/D ratio) in a buffer solution (at pH 4) containing 4 mM of the correspondent antipode and by using the oligo-(*R*)-BTIndT$_4$ modified electrode. Once again, during DOPA oxidation on the bare GC's surface, a well-defined peak, around 0.7 V versus Ag/AgCl, was observed (Figure S10a). However, when using the oligo-(*R*)-BTIndT$_4$ modified electrode, a peak-to-peak separation between the D- and L-enantiomers of 300 mV was obtained (Figure S10b). This observation indicates that the oligo-(*R*)-film inhibits the oxidation of L-DOPA; thus, an unfavorable diastereomeric interaction occurs. These results allow us to conclude that the enhancement or inhibition of the electron transfer is intimately related to the nature of the chiral analyte and the inherently chiral oligomer. Nonetheless, the peak-to-peak separation values obtained with the BTIndT$_4$ films agree with those obtained for the identical chiral probes using BT$_2$T$_4$ or 3,3′-bis(2,2′-bithiophen-5-yl)-1,1′-dimethyl-1*H*,1′*H*-2,2′-biindole (nicknamed (N-Me-IND)$_2$-T$_4$) films [42]. In fact, by comparing the enantioselective capabilities of these three inherently chiral oligomers toward the enantiomers of DOPA, BTIndT$_4$ exhibits the larger peak-to-peak separation (300 mV), demonstrating that the synergy between the two cores enhances the enantioselectivity of the oligomeric surface.

4 | Conclusion

In conclusion, we successfully synthesized a novel inherently chiral oligomer based on an indole–thianaphthene core with relatively high yields. The resulting compound coexists in two enantiomeric forms, and its corresponding separation was achieved via enantioselective HPLC. The indole moiety within the monomeric structure provides additional stability for the electrogenerated radical cations. These guide the oligomerization, producing well-ordered polymeric matrices, as the obtained quasimirror voltammetric signal demonstrates. The in situ electrochemical conductance study indicates that during the charge/discharge process, intrachain and interchain charge carriers' mobility occurs simultaneously. Finally, the enantioselective capabilities of the antipodes of the oligo-BTIndT$_4$ were demonstrated by the differentiation in terms of thermodynamic peak potential changes. In particular, this material inhibits the electron transfer process when unfavorable diastereomeric interaction occurs. Furthermore, in comparison with BT$_2$T$_4$ and (N-Me-IND)$_2$-T$_4$, the synergy between the two cores within BTIndT$_4$ enhances the enantioselectivity of the oligomeric surface.

Acknowledgments

This work has been funded by the H2020 European Research Council (ERC) under the HORIZON-ERC-2021 work program (grant agreement no. 101040798, ERC Starting grant CHEIR).

Mass spectrometry analyses were performed at the MS facility of the Unitech COSPECT at the University of Milan (Italy).

Data Availability Statement

The data that support the findings of this study are available on request from the corresponding author.

References

1. K. Namsheer and C. S. Rout, "Conducting Polymers: A Comprehensive Review on Recent Advances in Synthesis, Properties and Applications," *RSC Advances* 11 (2021): 5659–5697.

2. J. G. Ibanez, M. E. Rincon, S. Gutierrez-Granados, M. Chahma, O. A. Jaramillo-Quintero, and B. A. Frontana-Uribe, "Conducting Polymers in the Fields of Energy, Environmental Remediation, and Chemical–Chiral Sensors," *Chemical Reviews* 118 (2018): 4731–4816.

3. G. Salinas and B. A. Frontana-Uribe, "Electrochemical Analysis of Heavy Metal Ions Using Conducting Polymer Interfaces," *Electrochemistry* 3 (2022): 492–506.

4. J. Chung, A. Khot, B. M. Savoie, and B. W. Boudouris, "100th Anniversary of Macromolecular Science Viewpoint: Recent Advances and Opportunities for Mixed Ion and Charge Conducting Polymers," *ACS Macro Letters* 9 (2020): 646–655.

5. P. S. Sharma, M. Dabrowski, F. D'Souza, and W. Kutner, "Surface Development of Molecularly Imprinted Polymer Films to Enhance Sensing Signals," *Trends in Analytical Chemistry* 51 (2013): 146–157.

6. M. Dabrowski, M. Cieplak, K. Noworyta, et al., "Surface Enhancement of a Molecularly Imprinted Polymer Film Using Sacrificial Silica Beads for Increasing l-Arabitol Chemosensor Sensitivity and Detectability," *Journal of Materials Chemistry B* 5 (2017): 6292–6299.

7. J. Kalecki, M. Cieplak, Z. Iskierko, et al., "Post-Imprinting Modification: Electrochemical and Scanning Electrochemical Microscopy Studies of a Semi-Covalently Surface Imprinted Polymer," *Journal of Materials Chemistry B* 11 (2023): 1659–1669.

8. M. Cieplak and W. Kutner, "Artificial Biosensors: How Can Molecular Imprinting Mimic Biorecognition?" *Trends in Biotechnology* 34 (2016): 922–941.

9. M. Dabrowski, S. Reculusa, D. Thuau, C. Ayela, and A. Kuhn, "Macroporous Polymer Cantilever Resonators for Chemical Sensing Applications," *Advanced Materials Technologies* 8 (2023): 2300771.

10. C. D. McTiernan, K. Omri, and M. Chahma, "Chiral Conducting Surfaces via Electrochemical Oxidation of l-Leucine-Oligothiophenes," *Journal of Organic Chemistry* 75 (2010): 6096–6103.

11. C. McTiernan and M. Chahma, "Chiral Conducting Surfaces Based on the Electropolymerization of 3,4-Ethylenedioxythiophene," *Synthetic Metals* 161 (2011): 1532–1536.

12. Y. S. Jeong and K. Akagi, "Control of Chirality and Electrochromism in Copolymer-Type Chiral PEDOT Derivatives by Means of Electrochemical Oxidation and Reduction," *Macromolecules* 44 (2011): 2418–2426.

13. L. Dong, L. Zhang, X. Duan, D. Mo, J. Xu, and X. Zhu, "Synthesis and Characterization of Chiral PEDOT Enantiomers Bearing Chiral Moieties in Side Chains: Chiral Recognition and Its Mechanism Using Electrochemical Sensing Technology," *RSC Advances* 6 (2016): 11536–11545.

14. L. Dong, Y. Zhang, X. Duan, X. Zhu, H. Sun, and J. Xu, "Chiral PEDOT-Based Enantioselective Electrode Modification Material for Chiral Electrochemical Sensing: Mechanism and Model of Chiral Recognition," *Analytical Chemistry* 89 (2017): 9695–9702.

15. W. Gong, Z. Chen, J. Dong, Y. Liu, and Y. Cui, "Chiral Metal–Organic Frameworks," *Chemical Reviews* 122 (2022): 9078–9144.

16. N. Shukla and A. J. Gellman, "Chiral Metal Surfaces for Enantioselective Processes," *Nature Materials* 19 (2020): 939–945.

17. C. Wattanakit, "Chiral Metals as Electrodes," *Current Opinion in Electrochemistry* 7 (2018): 54–60.

18. W. Qi, C. Ma, Y. Yan, and J. Huang, "Chirality Manipulation of Supramolecular Selfassembly Based on the Host-Guest Chemistry of Cyclodextrin," *Current Opinion in Colloid & Interface Science* 56 (2021): 101526.

19. X. Niu, X. Yang, H. Li, J. Liu, Z. Liu, and K. Wang, "Application of Chiral Materials in Electrochemical Sensors," *Microchimica Acta* 187 (2020): 676.

20. O. I. Kalchenko, O. O. Trybrat, O. A. Yesypenko, V. V. Dyakonenko, S. V. Shishkina, and V. I. Kalchenko, "Inherently Chiral Dialkyloxy-Calix[4]Arene Acetic Acids as Enantiodiscriminating Additives for High-Performance Liquid Chromatography Separation of d,l-Amino Acids," *Chirality* 33 (2021): 722–730.

21. A. Gogoi, N. Mazumder, S. Konwer, H. Ranawat, N. T. Chen, and G. Y. Zhuo, "Enantiomeric Recognition and Separation by Chiral Nanoparticles," *Molecules* 24 (2019): 1007.

22. F. Sannicolo, S. Arnaboldi, T. Benincori, et al., "Potential-Driven Chirality Manifestations and Impressive Enantioselectivity by Inherently Chiral Electroactive Organic Films," *Angewandte Chemie, International Edition* 53 (2014): 2623–2627.

23. S. Luca, S. Grecchi, S. Rossi, et al., "Modulating the Enantiodiscrimination Features of Inherently Chiral Selectors by Molecular Design: A HPLC and Voltammetry Study Case With Atropisomeric 2,2'-Biindole-Based Monomers and Oligomer Films," *Chemistry - A European Journal* 27 (2021): 13190–13202.

24. S. Arnaboldi, S. Cauteruccio, S. Grecchi, et al., "Thiahelicene-Based Inherently Chiral Films for Enantioselective Electroanalysis," *Chemical Science* 10 (2019): 1539–1548.

25. C. Malacrida, L. Scapinello, R. Cirilli, et al., "In Situ Electrochemical Investigations of Inherently Chiral 2,2′-Biindole Architectures With Oligothiophene Terminals," *ChemElectroChem* 8 (2021): 3250–3261.

26. F. Sannicolò, S. Rizzo, T. Benincori, et al., "An Effective Multipurpose Building Block for 3D Electropolymerisation: 2,2′-Bis(2,2′-Bithiophene-5-Yl)-3,3′-Bithianaphthene," *Electrochimica Acta* 55 (2010): 8352–8364.

27. S. Arnaboldi, T. Benincori, R. Cirilli, et al., "Inherently Chiral" Thiophene-Based Electrodes at Work: A Screening of Enantioselection Ability Toward a Series of Pharmaceutically Relevant Phenolic or Catecholic Amino Acids, Amino Esters, and Amine," *Analytical and Bioanalytical Chemistry* 408 (2016): 7243–7254.

28. S. Arnaboldi, S. Grecchi, M. Magni, and P. R. Mussini, "Electroactive Chiral Oligo- and Polymer Layers for Electrochemical Enantiorecognition," *Current Opinion in Electrochemistry* 7 (2018): 188–199.

29. G. Salinas, F. Malacarne, G. Bonetti, et al., "Wireless Electromechanical Enantio-Responsive Valves," *Chirality* 35 (2023): 110–117.

30. S. Arnaboldi, G. Salinas, G. Bonetti, et al., "Autonomous Chiral Microswimmers With Self-Mixing Capabilities for Highly Efficient Enantioselective Synthesis," *Angewandte Chemie, International Edition* 61 (2022): e202209098.

31. G. Salinas and B. A. Frontana-Uribe, "Analysis of Conjugated Polymers Conductivity by In Situ Electrochemical-Conductance Method," *ChemElectroChem* 6 (2019): 4105–4117.

32. T. M. Swager, "Conducting/Semiconducting Conjugated Polymers. A Personal Perspective on the Past and the Future," *Macromolecules* 50 (2017): 4867–4886.

33. V. Bocchi and G. Palla, "High Yield Selective Bromination and Iodination of Indoles in N,N-Dimethylformamide," *Synthesis* 12 (1982): 1096–1097.

34. Y. Zou, G. Yue, J. Xu, and J. Zhou, "General Suzuki Coupling of Heteroaryl Bromides by Using Tri-Tert-Butylphosphine as a Supporting Ligand," *European Journal of Organic Chemistry* 27 (2014): 5901–5905.

35. J. S. Bair and R. G. Harrison, "Synthesis and Optical Properties of Bifunctional Thiophene Molecules Coordinated to Ruthenium," *Journal of Organic Chemistry* 72 (2007): 6653–6661.

36. T. Zheng, J. Xu, S. Cheng, J. Ye, S. Ma, and R. Tong, "Green Halogenation of Indoles With Oxone–Halide," *Journal of Organic Chemistry* 88, no. 16 (2023): 11497–11503.

37. G. Salinas, J. G. Ibanez, R. Vasquez-Medrano, and B. A. Frontana-Uribe, "Electrochemical Behavior of Poly-Bithiophene, Poly-3,4-Ethylendioxythiophene and Poly-3,4-Ortho-Xylendioxythiophene in EtOH/H2O (1:1) Mixture," *Synthetic Metals* 237 (2018): 65–72.

38. T. Benincori, S. Gamez-Valenzuela, M. Goll, et al., "Electrochemical Studies of a New, Low-Band Gap Inherently Chiral Ethylenedioxythiophene-Based Oligothiophene," *Electrochimica Acta* 284 (2018): 513–525.

39. J. Heinze, B. A. Frontana-Uribe, and S. Ludwigs, "Electrochemistry of Conducting Polymers-Persistent Models and New Concepts," *Chemical Reviews* 110 (2010): 4724–4771.

40. T. Nicolini, A. V. Marquez, B. Goudeau, A. Kuhn, and G. Salinas, "In Situ Spectroelectrochemical-Conductance Measurements as an Efficient Tool for the Evaluation of Charge Trapping in Conducting Polymers," *Journal of Physical Chemistry Letters* 12 (2021): 10422–10428.

41. S. Grecchi, G. Salinas, R. Cirilli, et al., "Miniaturized Enantioselective Tubular Devices for the Electromechanical Wireless Separation of Chiral Analytes," *Chem* 10 (2024): 660–674.

42. S. Arnaboldi, T. Benincori, A. Penoni, et al., "Highly Enantioselective "Inherently Chiral" Electroactive Materials Based on a 2,2′-Biindole Atropisomeric Scaffold," *Chemical Science* 10 (2019): 2708–2717.

Supporting Information

Additional supporting information can be found online in the Supporting Information section.